Energy &
Environmental
Science

A Novel Low-Thermal-Budget Approach for Co-Production of Ethylene and Hydrogen via Electrochemical Non-Oxidative Deprotonation of Ethane

SCHOLARONE™
Manuscripts

Journal Name

ARTICLE

A Novel Low-Thermal-Budget Approach for Co-Production of Ethylene and Hydrogen via Electrochemical Non-Oxidative Deprotonation of Ethane

Dong Ding,*[a] Yunya Zhang,[a] Wei Wu,[a] Dongchang Chen,[b] Meilin Liu[b] and Ting He*[a]

The oversupply of ethane, a major component of natural gas liquids, has stimulated the wide applications of ethylene since the shale gas evolution. However, ethylene production is energy-intensive and represents the most energy-consuming single process in chemical industry. In this paper, we report, for the first time, a novel low-thermal-budget process for the co-production of ethylene and pure hydrogen using a proton-conducting electrochemical deprotonation cell. At a constant current density of 1 A cm^{-2}, corresponding to a hydrogen production rate of 0.448 mol cm^{-2} per day, and 400 °C, a close to 100% ethylene selectivity was achieved under an electrochemical overpotential of 140 mV. Compared to the industrial ethane steam cracker, the electrochemical deprotonation process can achieve a 65% in process energy saving and reduce the carbon footprint by as much as 72% or even more if renewable electricity and heat are used. If the heating value of produced hydrogen is taken into account, the electrochemical deprotonation process actually has a net gain in processing energy. The electrochemical deprotonation process at reduced temperatures in the present study provides a disruptive approach for petrochemical manufacturing, shifting the paradigm from thermal chemical practice to a clean energy regime.

Introduction

Ethylene, one of the largest building blocks in petrochemical industry, is primarily used in the production of polymers and their derivatives. It reached an over 143 million tons yearly production worldwide in 2012.[1] The predominant manufacturing routes by far are thermal cracking of ethane (gas) and naphtha (liquid) feedstocks in the presence of steam (steam cracking). While naphtha steam cracking remains prevalent in Asian and European markets, the global share of ethane has grown drastically in recent years, especially in the United States and Middle East. This shift in emphasis from naphtha to ethane has been driven largely by the cheaper price of ethane (18 cents per gallon[2]) due to its oversupply since the shale gas revolution. Typically the steam cracking of ethane has a conversion rate of 70%, with ethylene yields of about 50%.[3] However, steam cracking is energy-intensive and represents the most energy-consuming single process in chemical industry.[4, 5] For example, ethane steam cracking consumes typically 17-21 GJ (specific energy consumption, SEC) of process energy per ton of ethylene,[6] of which 65% is used in high temperature pyrolysis, 15% in fractionation and compression, and 20% in product separation.[7, 8] It is estimated that the steam cracking process contributes 60% of the product cost and two-thirds of the manufacturing carbon

footprint.

In addition to the matured industrial ethane steam cracking, catalytic dehydrogenation of ethane has emerged by adopting highly selective catalysts such as Pt, Pd or CrO$_x$.[9] Because of the thermodynamic limitation, in particular for light carbon compounds,[10] ethane conversion was greatly restrained. For example, the conversion was reported to be ~15% at 600 °C[11-13] and no more than 40% at 650-700 °C.[14, 15] This can be compensated by operation at higher temperatures, but side reactions, coke formation and catalyst deactivation are also accelerated.[16]

To improve the conversion at reduced temperatures, oxidative dehydrogenation (oxydehydrogenation, ODH) of ethane was proposed.[17] The conversion in ODH is theoretically close to unit and could bring up the potential energy saving of approximate 35%.[6] Unfortunately, the choice of the catalysts limited its further market penetration to realize "true" ODH,[18-20] especially due to the fact that the product subjecting to catalyst surfaces is often oxidized more easily than the feedstock. As a result, it requires operating the process at low conversions in order to reach high selectivity.[21, 22] It seems to be a paradox unless highly selective catalysts can be discovered.[23] Moreover, the relatively low energy efficiency, higher CO$_2$ emission and additional safety consideration are other major challenges when those variables, such as oxygen production and usage, and product combustion are taken into account.[6, 24] To achieve significant progress in the reduction of both processing energy and carbon footprint, simple process optimization may not be sufficient owing to the maturity of the manufacturing industry (centralized and vertical integrated), where materials and energy efficiencies have been extensively optimized with a long track

[a.] Energy & Environment Science and Technology, Idaho National Laboratory, Idaho Falls, ID 83415 USA. E-mail address: dong.ding@inl.gov; ting.he@inl.gov
[b.] School of Materials Science & Engineering, Georgia Institute of Technology, Atlanta, GA 30332 USA.
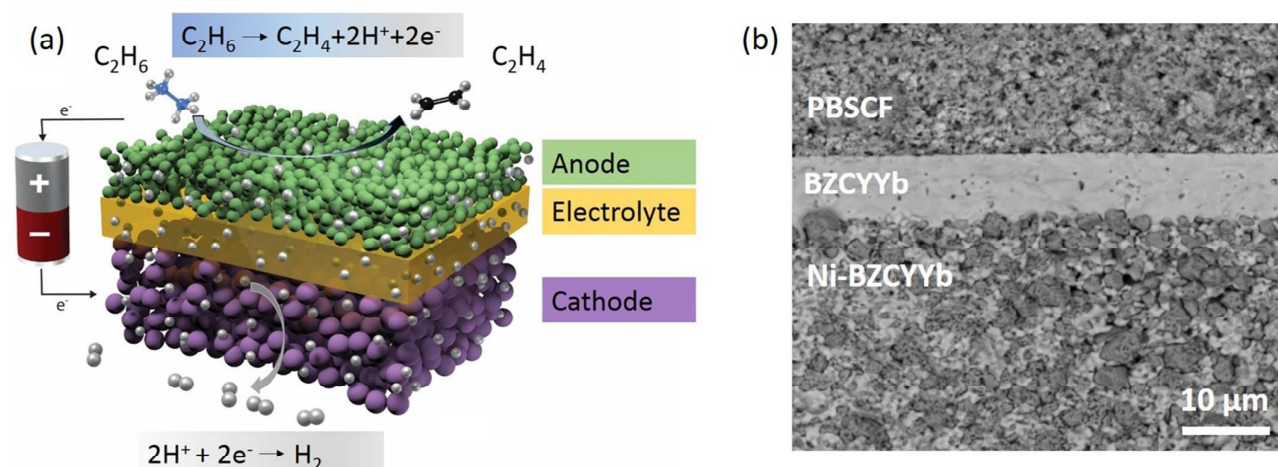
Figure 1. Non-oxidative deprotonation process (NDP) and cell illustration. (a) Schematic of the co-production of ethylene and hydrogen via an NDP process of ethane in a proton conducting electrochemical cell. Ethane was fed into in the anode and deprotonated to produce ethylene and protons, which transferred through the electrolyte membrane to cathode and combined with electrons, and eventually formed hydrogen. (b) A cross-sectional SEM image of an actual electrochemical cell after test at 400 ^{o}C. Porous BZCYYb-Ni anode (300 μm) supported BZCYYb electrolyte (10 μm) with a porous layer of PBSCF cathode on the top (30 μm).

record of reliable operation. Therefore, it is vital to develop disruptive methods that are both low-thermal-budget (LTB) and low-carbon-footprint (LCF), aiming to fully exploit the potential of ethane as a feedstock.[25]

Apart from the search for better catalysts for catalytic dehydrogenation, hydrogen permeation membranes were also used to overcome the thermodynamic limit. For example, a thick $SrCe_{0.95}Yb_{0.05}O_{3-\delta}$ membrane was used for dehydrogenation of ethane at 700 ^{o}C[26] and methane at 900 ^{o}C.[27] Recently, Luo et al. reported the co-generation of electricity and ethylene using a proton conducting electrolyte based solid oxide fuel cell (SOFC) with ethane as feedstock.[28, 29] Using a Co-Fe alloy anode catalyst, the ethane conversion increased from 13.5 to 45.4% when the temperature was increased from 650 to 750 °C where ethylene selectivity was as high as 91%.[30] Nevertheless, it should be noted that the proton conductors are actually a mixed oxygen-ion and proton conductor above 600 °C,[31] so it can be considered an ODH process again. In addition, coking and fast degradation remain challenging at high operating temperatures.[32-34] In fact, the concept of using protonic and oxygen ionic mixed conductors has been successfully applied for converting methane into aromatic chemicals at ~700 °C.[35]

In this paper, we report an innovative approach to circumvent the current limitation of ethylene production by shifting the petrochemical manufacturing paradigm from widely used thermal practices to a clean energy regime. Specifically, we have developed a pure proton-conducting electrochemical cell for the co-production of ethylene and hydrogen via electrochemical non-oxidative deprotonation (NDP) of ethane (400-500 ^{o}C). The electrochemical cell consisted of a superior proton-conducting electrolyte thin film,

a porous anode support and a porous cathode. Ethane was fed to the anode and electrochemically deprotonated into ethylene and protons when an electrical field was applied. The generated protons transferred through the dense proton-conducting membrane to the cathode where they combined with electrons and formed high-purity hydrogen. Figure 1(a) is a schematic drawing of the reaction principle and the configuration of the electrochemical cell. The rate of the reaction was controlled by the flux of protons passing through the electrolyte, the kinetics of ethane oxidation reaction (e.g., deprotonation), and hydrogen evolution reaction. The flux of protons (H^+), J_{H+}, was controlled by the applied voltage across the membrane:

$$J_{H^+} = -\frac{D_H C_H}{RT} z_H F \cdot \nabla(\mu_H + z_H F\varphi)$$

where D, C, z, μ, φ, F, R and T are the diffusion coefficient, concentration, charge number, chemical potential, electrical potential, Faraday constant, gas constant, and temperature, respectively.

The electrolyte of the electrochemical NDP cells is acceptor-doped barium zirconate cerate ($BaZr_{0.1}Ce_{0.7}Y_{0.1}Yb_{0.1}O_{3-\delta}$, BZCYYb),[36] which exhibits ionic conductivity as high as 6.2×10^{-3} S cm^{-1} at 400 ^{o}C with a small activation energy (Figure. S1). In addition, this type of materials has a very high proton transfer number at temperatures lower than 550 ^{o}C,[37] allowing pure proton conduction at high flux under reduced operating temperatures,[38] where coking is restrained thermodynamically. A fully assembled cell consisted of a dense 10 μm-thick BZCYYb electrolyte thin film on a porous BZCYYb-Ni anode support (300 μm), and a porous double perovskite $PrBa_{0.5}Sr_{0.5}Co_{1.5}Fe_{0.5}O_{5+\delta}$ (PBSCF) layer (30 μm) as a cathode (Figure

1(b)). Ni is an excellent catalyst for ethane oxidation reaction [39, 40], and the PBSCF family has been demonstrated to be triple-conducting materials ($H^+/O^{2-}/e^-$),[41] which has good activity for hydrogen evolution reactions.

Methods

Powder synthesis

$BaZr_{0.1}Ce_{0.7}Y_{0.1}Yb_{0.1}O_{3-\delta}$ (BZCYYb) powder used for electrolyte and anode was prepared by solid state reaction from stoichiometric precursors barium carbonate (Sigma Aldrich, ≥99%, $BaCO_3$), zirconium oxide (Alfa Aesar, 99%, ZrO_2), cerium(IV) oxide (Aldrich, 99.9%, CeO_2), yttrium(III) oxide (Alfa Aesar, 99.99%, Y_2O_3), and ytterbium(III) oxide (Alfa Aesar, 99.9%, Yb_2O_3). The powder was ball-milled for 24 h in ethanol, dried for 24 h, crushed, and calcined at 1100 °C for 10 h. The process was repeated to achieve a pure perovskite phase. The $PrBa_{0.5}Sr_{0.5}Co_{1.5}Fe_{0.5}O_{5+\delta}$ (PBSCF) cathode material was synthesized by a glycine-nitrate process (GNP). Stoichiometric amounts of $Pr(NO_3)_3·6H_2O$ (Alfa Aesar, 99.9%, metal basis), $Ba(NO_3)_2$ (Alfa Aesar, 99.95%), $Sr(NO_3)_2$ (Alfa Aesar, 99.97%), $Co(NO_3)_2·6H_2O$ (Aldrich, 98+%) and $Fe(NO_3)_3·9H_2O$ (Alfa Aesar, 98+%) were dissolved in distilled water with proper amount of glycine. The solution was heated up to 350 °C in air and followed by combustion to form fine powder which was calcined at 600 °C for 4 h. The resulting powder was then grinded and calcined again at 900 °C for 4 h.

Electrochemical cell fabrication

Button cells with a configuration of NiO-BZCYYb|BZCYYb|PBSCF were fabricated by a standard procedure. Firstly, a mixture of NiO (Alfa Aesar) and BZCYYb powder (weight ratio of 60:40) was mixed in ethanol and toluene using a high-energy ball mill (SPEX, 8000M) for 20 min. Plastizers and binders were added and then mixed for another 20 min to obtain a slip, which was degased and tape-casted to form green tapes. After drying overnight, the green tape was punched into wafers (12.7 mm in diameter), followed by pre-firing at 950 °C for 2 h forming anode supports (~0.3 mm thick). Secondly, a thin layer of BZCYYb (~10 μm) was deposited on the anode
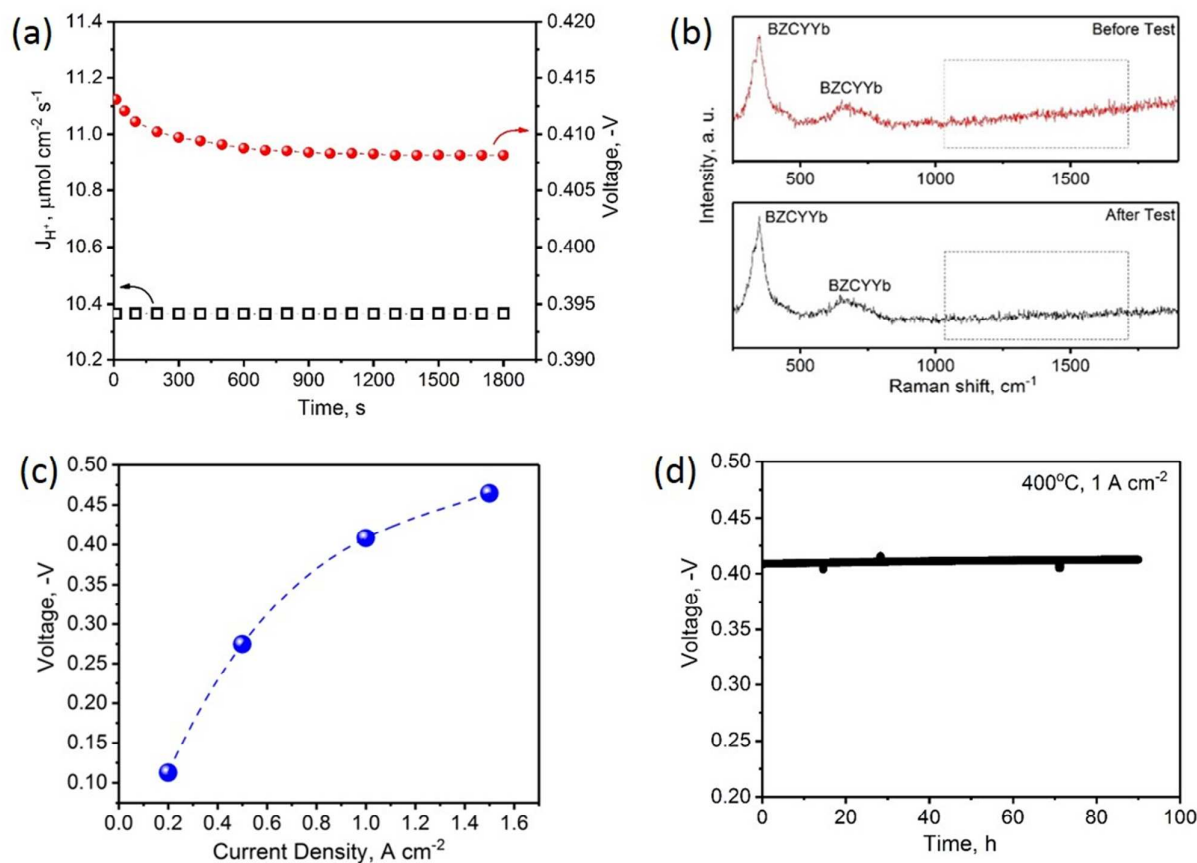

Figure 2. NDP performance with 10% ethane in Ar at 400 °C. (a) Proton flux and the corresponding voltage of the electrochemical cell at a constant current density of 1 A cm^{-2} as a function of time. An overpotential of 0.140 V was observed when the steady state was reached. (b) *Ex-situ* Raman spectra of the anode in the electrochemical cell before (upon reduction) and after test at 400 °C. Raman bands of carbonaceous species were not detected, which normally appeared in the dashed rectangular area. (c) Voltage responses to the applied constant current density of 0.2, 0.5, 1.0, and 1.5 A cm^{-2}. The data point was collected when the steady state was reached at each current density. (d) Durability test at a constant current density of 1 A cm^{-2}. The stable voltage output over 90 h suggested durable operation.

support by a slurry coating process followed by co-firing at 1400 ^{o}C for 4 h.[42] Thirdly, a PBSCF ink was screen printed onto the top of the BZCYYb electrolyte and fired at 900 ^{o}C for 2 h to form a porous cathode. The active electrode area for all cells is 0.32 cm^2 (Figure S3(a)).

Characterization

The phase purity of the BZCYYb electrolyte, NiO-BZCYYb anode and PBSCF cathode was examined with a Rigaku SmartLab X-Ray Diffraction (XRD) in 20-90° angular range with a step of 0.04° and a resonance time of 1.6 s. The total conductivity of the BZCYYb electrolyte was measured in air between 400–650 °C using an electrochemical impedance spectroscopy (EIS) from Solartron (1400 Cell Test System). The microstructure of the electrochemical cell was characterized either via SEM (JEOL 6700F) equipped with a back scattering electron (BSE) analyser, or transmission electron microscope (TEM) equipped with energy dispersive x-ray spectroscopy (JEOL 4000 EX). Raman spectroscopic measurement was performed with a Renishaw RM1000 micro-spectrometer using a Melle-Griot Ar-ion Laser with a wavelength of 514 nm. *In-situ* Raman measurements were performed using a pre-designed high temperature cell.

Performance Testing

The electrochemical cell was sealed in a home-made reactor (Figure S3(b)) using glass sealant (Schott, Germany). Silver mesh and Platinum wire were used as the current collector and leads, respectively. A thermal couple was placed in the reactor to monitor the cell temperature. The cell was ramped up to 750 ^{o}C for 30 min and the temperature was then reduced to 500 ^{o}C during testing. Air (30 mL min^{-1}) was used during ramping up and pure hydrogen, with a flow rate of 10 mL min^{-1}, was switched in to reduce NiO to Ni at or above 600 ^{o}C. For each testing temperature, Ar was first swept in the anode to flush out hydrogen, and different concentrations of ethane (1%, 5%, 10%, 50% and 100%) in Ar was purged as feedstock. In the cathode, pure oxygen was switched to pure Ar as the sweeping gas. The electrochemical NDP process started when a fixed current density. The corresponding voltage was recorded over time. Gas compositions at both sides were analyzed using gas chromatography (GC, Shimadzu 2010 plus) at open circle voltage as well as when the voltage become stable.

Results and discussion

Electrochemical performance and product selectivity

The electrochemical NDP was carried out at 400 and 500 ^{o}C with ethane as feedstock. As shown in Figure 2(a), a constant current density of 1 A cm^{-2} was applied to the cell when 10% ethane in Ar was introduced. This corresponded to a proton flux of 10.37 μmol cm^{-2} s^{-1} or a hydrogen production rate of 0.448 mol cm^{-2} per day, which was confirmed by gas chromatography (GC) analysis on the cathode side (Detailed GC data and corresponding calculations are shown in SI). At 400 ^{o}C, the Gibbs free energy of the following reaction is 51.7 kJ mol^{-1}, which is equivalent to a thermodynamic potential of -0.268 V.

$$C_2H_6 \rightleftharpoons C_2H_4 + H_2$$
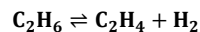
The recorded voltage approached a constant value of -0.408 V in about 20 min, implying that a steady state had been reached. The overpotential under the condition was calculated to be only 0.140 V. According to the conductivity of BZCYYb (Figure S1), the Ohmic overpotential associated with the electrolyte was 0.083 V while the overpotential contributed by electrode reactions was 0.057 V, including ethane oxidation reaction (EOR) and hydrogen evolution reaction (HER). The low overpotential demonstrated a successful assembly of the high-performing electrochemical cell and a small electrical energy consumption.

In order to quantify the ethylene selectivity, an online GC analysis was employed to analyze the gaseous products of the electrochemical NDP. In our present study, the most possible products containing carbon species were ethylene, methane and acetylene. GC results indicated that the gaseous products were free of both acetylene and methane. In addition, both *ex-situ* and *in-situ* Raman spectroscopic measurements were performed to identify coke formation, which has been proven a powerful technique due to its chemical and surface sensitivity.[43, 44] Figure 2(b) shows the *ex-situ* Raman spectra of the anode in the electrochemical cell before and after NDP testing at 400 ^{o}C. The Raman bands at the low wavenumber region correspond to the vibration bands of BZCYYb and agree well with those reported previously.[45] It is obvious that no Raman band of carbonaceous species appeared in the cell after test, as marked in the dashed region. This was further confirmed by *in-situ* Raman spectroscopy in a predesigned in-situ cell where the cell was exposed to ethane for 45 min with an interval of 90 s (Figure S4). These results concluded that the selectivity was close to 100%.

The relationship between current density and voltage was investigated to unveil the effect of input electrical energy on the reaction rate. As shown in Figure 2(c), the voltages are -0.113, -0.275, -0.408, and -0.465 V at the current density of 0.2, 0.5, 1.0, and 1.5 A cm^{-2}, respectively, when a steady state was reached at each current density. The total cell resistance, calculated from V/I, tended to decrease with increasing current density. Further investigation, along with electrochemical impedance spectrum, will help to gain more insight into the reaction mechanism and rate-limiting steps.

A long-term stability test was performed to confirm the durability of the electrochemical NDP as well as the materials used in the present study. Figure 2(d) shows the voltage response at a constant current density of 1 A cm^{-2} with a 10% ethane in Ar for over 90 h. The voltage fluctuated slightly in the range of -0.407 and -0.413 V, suggesting good durability under the operating conditions. This is also consistent with our Raman observation.

It should be noted that the small overpotential was also demonstrated with the identical current density at 500 ^{o}C (Figure S5). However, the selectivity was expected to be decreased at 500 ^{o}C due to the coking formation, which was observed both visually and by Raman analysis (Figure S5). The increase in intensities of carbon D and G bands of the Raman spectra implies an increase in the degree of coking as the temperature was increased from 450 ^{o}C to 500 ^{o}C under the operation conditions. The results suggested
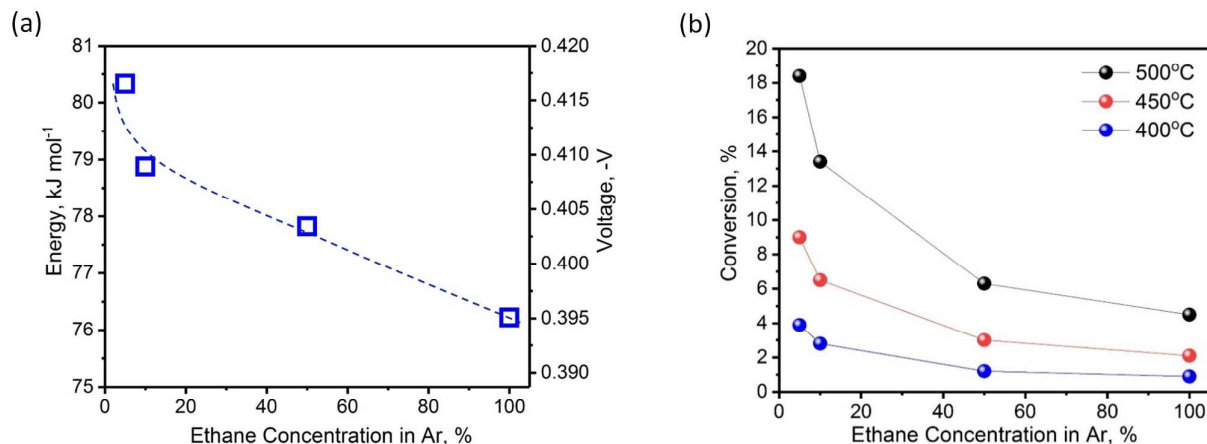
Figure 3. Energy input *vs*. ethane concentration in NDP and Conversion *vs*. ethane concentration in thermal cracking. (a) The cell voltage and corresponding energy input at a constant current density of 1 A cm^{-2} when equilibrated as a function of ethane concentration. The energy input decreases with the increasing concentration of ethane, indicating that NDP favors a higher ethane concentration in terms of energy consumption. (b) The calculated equilibrium conversion of ethane into ethylene as a function of ethane concentration at a constant pressure of 1 atm at 400-500 ^{o}C. The ethane conversion decreases with increasing ethane concentration, implying lower concentration is preferable with respect to the conversion in the process of the thermal cracking.

that the thermodynamic cracking of ethane into carbon was greatly inhibited when the temperature was reduced from 500 to 400 ^{o}C, implying the significance of reducing operating temperatures in improving ethylene selectivity. It is further noted that hydrogen was not detectable in the anode compartment when the cell was at open circuit voltage or under operation, indicating that the catalytic dehydrogenation of ethane was minimal at 400 ^{o}C.

The relationship between the energy consumption and the ethane concentration was depicted in Figure 3(a). The former was converted from recorded electrical voltages under equilibrium. The voltage dropped from -0.417 V to -0.395 V, which equaled to a decrease in the energy input from 80.3 kJ mol^{-1} to 76.2 kJ mol^{-1}, when the ethane concentration increased from 5% to 100% while the proton flux was fixed. This indicates that the electrochemical

NDP favors higher ethane concentration, whereas the ethane thermal-cracking favors lower ethane concentration,[46] as shown in Figure 3(b). For example, the conversion was reduced from 3.9% at 5% ethane to 0.9% at 100% ethane at 400 ^{o}C.

Comparison of process energy and CO$_2$ emission in NDP and ethane steam cracker

Based on the results at 400 ^{o}C, Figure 4(a) shows a comparison of the process energies required in our electrochemical NDP to the industrial steam cracking in ethylene production (in kJ per mole of ethylene), where ΔH and ΔG are enthalpy and Gibbs free energy, respectively, for the ethane conversion to ethylene and hydrogen. The industrial energy consumption from steam cracking was taken from a 2006 report, the newest publicly available and widely cited
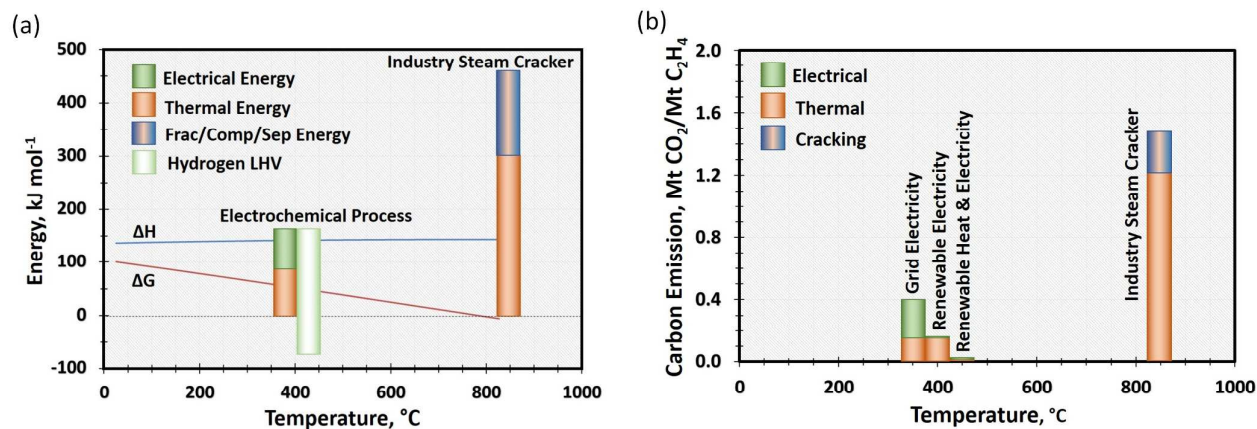

Figure 4. Comparison of process energies and carbon footprint in NDP and steam cracking. (a) A comparison of the process energies for ethylene production from ethane. (b) A comparison of the carbon footprint for ethylene production from ethane. The NDP was carried out at 400 °C whereas the steam cracking was performed at 850 °C.

data.[6, 7] The typical SEC was 17-21 GJ per ton of ethylene. For simplification, the smallest energy consumption of 17 GJ per ton of ethylene production was used for comparison, of which 65% was thermal energy requirement and 35% for fractionation, compression and separation. As a contrast, our thermal and electrical energy consumptions, derived from the results above, were 3.2 and 2.8 GJ per ton of ethylene, respectively (for details, see the breakdown of process energy consumption calculation in the Supporting Information). It clearly indicates that our electrochemical process has a 71% thermal energy saving and about 65% total energy saving compared to industrial steam cracking. If we take the heating value of generated hydrogen into account, the electrochemical NDP process actually has a net process energy gain. It is worth noting that hydrogen generated in the electrochemical process is pure, no further separation is needed, and can be directly used instead of being combusted as a waste in industrial steam cracking process due to its high separation cost.

The electrochemical NDP also has a remarkable advantage in reducing the carbon footprint. Figure 4(b) shows a comparison of CO_2 emission in our electrochemical process to the industrial steam cracking in ethylene production (detailed breakdown calculations are summarized in the Supporting Information). The steam cracking process emitted 0.27 tons of CO_2 per ton of ethylene, and fuel combustion and utilities accounted for 1.20 tons of CO_2 emissions per ton of ethylene, resulting in an 1.47 tons of CO_2 emission per ton of ethylene in total.[6] In electrochemical NDP, there were two primary contributors to the carbon footprint: CO_2 emission associated with the thermal energy supplied for ethane deprotonation and the electricity energy applied to the cell. The former gave a 0.15 tons CO_2 emission per ton of ethylene while the latter had a 0.25 tons CO_2 emission per ton of ethylene when the fossil based electricity was used. This led to an over 72% reduction in carbon footprint. Furthermore, it will result in an 89% reduction, or about one tenth of the carbon footprint of the industrial steam cracking, when renewable electricity (e.g. nuclear, wind and hydropower, which dominate U.S renewable energy supply[47]) is used. Eventually a 98% reduction in carbon footprint can be achieved when renewable energy is used for both heat and electricity.

In comparison to the thermochemical processes of ethylene production, our work has the following advantageous implications: (1) The electrochemical process has the capability of overcoming the thermodynamic limitation, allowing operation at a reduced temperature in order to mitigate challenges associated with side reactions, coke formation and catalyst deactivation, etc.; (2) as our experimental results demonstrated, the EOR and HER are low overpotential processes at the operating temperatures, requiring a relatively small electrical energy input and having a close to unit Faraday efficiency; and (3) the electrochemical NDP can also overcome the challenge of competitive reaction between feedstock and product, alleviate safety consideration and reduce the carbon footprint.

Conclusions

The co-production of ethylene and hydrogen has been successfully demonstrated through an electrochemical NDP process at 400 ^{o}C,

with an ethylene selectivity close to 100% and a hydrogen generation rate of 0.448 mol cm^{-2} per day. Compared to the commercial ethane steam cracking process, the NDP at the reduced operating temperature can achieve a ~65% reduction in process energy, and a 72% reduction in carbon footprint. Taking the estimated energy manufactured and serviced in the United States in 2016[48] as an example, 34% of the manufactured energy and 39% of the serviced energy were associated with industrial applications, of which the petrochemical industry consumed 42%. Given the intensity of energy consumption in this industry and relevant carbon footprint, as much as 6.4 quadrillion BTU of energy could be saved (65%) if such low-thermal-budget technologies can be widely deployed. Clearly, enabling advanced process innovation in the thermodynamic and electrical domains can be disruptive for changing the manufacturing infrastructure and in establishing new businesses that drive economic prosperity.

As an emerging technology, there exists opportunities to modify electrode catalysts and proton conduction in electrolytes to further reduce overpotential, i.e. the electrical energy consumption. Scaling-up of the electrochemical cells into the real reactor is ongoing to determine production and operation durability.

Conflicts of interest

The authors declare no competing financial interests.

Acknowledgements

References

1. W. R. True, *Global ethylene capacity poised for major expansion,* http://www.ogj.com/articles/print/volume-111/issue-7/special-report-ethylene-report/global-ethylene-capacity-poised-for-major.html, 2013.
2. ICIS, http://www.icis.com/resources/news/2016/09/06/10031804/fears-of-us-ethane-price-spike-overblown-analyst/, 2016.
3. H. Zimmermann and R. Walzl, in *Ullmann's Encyclopedia of Industrial Chemistry*, Wiley-VCH Verlag GmbH & Co. KGaA, 2000.
4. IEA, *Energy Statistics of OECD countries 2001/2002 and energy statistics of non-OECD countries 2001/2002 (2004 Edition). Paris: International Energy Agency*, 2004.
5. DOE, *Manufacturing Consumption Energy Survey. Washington DC: Energy Information Adminstration of the US Department of Energy.* , 1998.
6. T. Ren, M. Patel and K. Blok, *Energy*, 2006, **31**, 425-451.
7. V. Kaiser, J. Ruiz-Martinez, E. Santillan-Jimenez and B. M. Weckhuysen, *Ethylene plant energy analysis. National Meeting of AIChE*, Houston, 1993.

8.   E. Worrell, D. Phylipsen, D. Einstein and N. Martin, 2000.
9.   C. Coperet, *Chem Rev*, 2010, **110**, 656-680.
10.   M. M. Bhasin, J. H. McCain, B. V. Vora, T. Imai and P. R. Pujado, *Appl Catal A-gen*, 2001, **221**, 397-419.
11.   H. Yang, L. Y. Xu, D. C. Ji, Q. X. Wang and L. W. Lin, *React Kinet Catal L*, 2002, **76**, 151-159.
12.   J. Wu, S. M. Sharada, C. Ho, A. W. Hauser, M. Head-Gordon and A. T. Bell, *Appl Catal A-gen*, 2015, **506**, 25-32.
13.   Z. Wu, E. C. Wegener, H. T. Tseng, J. R. Gallagher, J. W. Harris, R. E. Diaz, Y. Ren, F. H. Ribeiro and J. T. Miller, *Catalysis Science & Technology*, 2016, **6**, 6965-6976.
14.   K. Nakagawa, M. Okamura, N. Ikenaga, T. Suzuki and T. Kobayashi, *Chem Commun*, 1998, 1025-1026.
15.   A. Tsyganok, P. J. E. Harlick and A. Sayari, *Catalysis Communications*, 2007, **8**, 850-854.
16.   H. J. Lugo and J. H. Lunsford, *J Catal*, 1985, **91**, 155-166.
17.   H. H. Kung, in *Advances in Catalysis, Vol 40*, eds. D. D. Eley, H. Pines and W. O. Haag, 1994, vol. 40, pp. 1-38.
18.   M. A. Banares, *Catal Today*, 1999, **51**, 319-348.
19.   J. L. Lu, B. S. Fu, M. C. Kung, G. M. Xiao, J. W. Elam, H. H. Kung and P. C. Stair, *Science*, 2012, **335**, 1205-1208.
20.   M. M. Bhasin, *Top Catal*, 2003, **23**, 145-149.
21.   J. A. Lercher and F. N. Naraschewski, *Nanostructured Catalysts-Selective Oxidation*, Royal Society of Chemistry, 2011.
22.   C. A. Gartner, A. C. van Veen and J. A. Lercher, *Chemcatchem*, 2013, **5**, 3196-3217.
23.   W. D. Pyrz, D. A. Blom, N. R. Shiju, V. V. Guliants, T. Vogt and D. J. Buttrey, *Catal Today*, 2009, **142**, 320-328.
24.   J.-P. Lange, *CATTECH*, 2001, **5**, 82-95.
25.   J. S. Plotkin, *Beyond the Ethylene Steam Cracker,* https://www.acs.org/content/acs/en/pressroom/cutting-edge-chemistry/beyond-the-ethylene-steam-cracker.html, 2016.
26.   T. Hibino, S. Hamakawa and H. Iwahara, *Nippon Kagaku Kaishi*, 1993, 238-242.
27.   S. Hamakawa, T. Hibino and H. Iwahara, *J Electrochem Soc*, 1993, **140**, 459-462.
28.   Z. C. Shi, J. L. Luo, S. Y. Wang, A. R. Sanger and K. T. Chuang, *J Power Sources*, 2008, **176**, 122-127.
29.   X. Z. Fu, J. L. Luo, A. R. Sanger, N. Danilovic and K. T. Chuang, *Chem Commun*, 2010, **46**, 2052-2054.
30.   S. B. Liu, K. T. Chuang and J. L. Luo, *Acs Catalysis*, 2016, **6**, 760-768.
31.   K. D. Kreuer, E. Schonherr and J. Maier, *Solid State Ionics*, 1994, **70**, 278-284.
32.   E. D. Wachsman and K. T. Lee, *Science*, 2011, **334**, 935-939.
33.   D. Ding, X. X. Li, S. Y. Lai, K. Gerdes and M. L. Liu, *Energy Environ Sci*, 2014, **7**, 552-575.
34.   S. McIntosh and R. J. Gorte, *Chem Rev*, 2004, **104**, 4845-4865.
35.   S. H. Morejudo, R. Zanon, S. Escolastico, I. Yuste-Tirados, H. Malerod-Fjeld, P. K. Vestre, W. G. Coors, A. Martinez, T. Norby, J. M. Serra and C. Kjolseth, *Science*, 2016, **353**, 563-566.
36.   L. Yang, S. Wang, K. Blinn, M. Liu, Z. Liu, Z. Cheng and M. Liu, *Science*, 2009, **326**, 126-129.
37.   K. D. Kreuer, W. Munch, M. Ise, T. He, A. Fuchs, U. Traub and J. Maier, *Berichte Der Bunsen-Gesellschaft-Physical Chemistry Chemical Physics*, 1997, **101**, 1344-1350.
38.   C. Duan, J. Tong, M. Shang, S. Nikodemski, M. Sanders, S.

Ricote, A. Almansoori and R. O'Hayre, *Science*, 2015, **349**, 1321-1326.
39.   A. Atkinson, S. Barnett, R. J. Gorte, J. T. S. Irvine, A. J. Mcevoy, M. Mogensen, S. C. Singhal and J. Vohs, *Nature Materials*, 2004, **3**, 17-27.
40.   W. Wang, C. Su, Y. Wu, R. Ran and Z. Shao, *Chem Rev*, 2013, **113**, 8104-8151.
41.   J. Kim, S. Sengodan, G. Kwon, D. Ding, J. Shin, M. L. Liu and G. Kim, *Chemsuschem*, 2014, **7**, 2811-2815.
42.   D. Ding, M. F. Liu, Z. B. Liu, X. X. Li, K. Blinn, X. B. Zhu and M. L. Liu, *Advanced Energy Materials*, 2013, **3**, 1149-1154.
43.   X. Li, J.-P. Lee, K. S. Blinn, D. Chen, S. Yoo, B. Kang, L. A. Bottomley, M. A. El-Sayed, S. Park and M. Liu, *Energy Environ. Sci.*, 2014.
44.   D. Chen, X. Xiong, B. Zhao, M. A. Mahmoud, M. A. El-Sayed and M. Liu, *Advanced Science*, 2016, **3**, 1500433.
45.   L. Yang, S. Wang, K. Blinn, M. Liu, Z. Liu, Z. Cheng and M. Liu, *Science*, 2009, **326**, 126-129.
46.   D. E. Resasco and G. L. Haller, in *Catalysis: Volume 11*, eds. J. J. Spivey and S. K. Agarwal, The Royal Society of Chemistry, 1994, vol. 11, pp. 379-411.
47.   EIA, https://www.eia.gov/outlooks/steo/report/renew_co2.cfm, 2017.
48.   L. L. N. Laboratory, *Estimated U.S. Energy Use in 2016,* https://flowcharts.llnl.gov/content/assets/images/energy/us/Energy_US_2016.png, 2016.

Broader Context

Ethylene, one of the largest building blocks in petrochemical industry, is primarily used in the production of polymers and their derivatives. The predominant manufacturing routes are steam thermal cracking of ethane and naphtha. The former has grown drastically in recent years, especially in the United States and Middle East due to cheap price of ethane since the shale gas revolution. However, ethylene production is energy-intensive and represents the most energy-consuming single process in chemical industry. Herein we demonstrated a concept feasibility for a low-thermal-budget and low-carbon-footprint electrochemical process for the co-production of ethylene and pure hydrogen. Compared to the industrial ethane steam cracking, the electrochemical process can achieve a 65% savings in process energy and reduce the carbon footprint by as much as 72% or even more if renewable electricity and heat are used. If the heating value of produced hydrogen is taken into account, it actually has a net gain in process energy. The success of this transformational technology can fundamentally change the petrochemical manufacturing paradigm from fossil energy fueled "thermal" practices to a "clean energy" scheme that incorporates renewable energies, leading to eventually industrial electrification.